Expansion of the fusion stalk and its implication for biological membrane fusion

Herre Jelger Risselada[a,b,1], Gregory Bubnis[a], and Helmut Grubmüller[a]

[a]Theoretical and Computational Biophysics Department, Max Planck Institute for Biophysical Chemistry, 37077 Göttingen, Germany; and [b]Leibniz Institute of Surface Modification, D-04318 Leipzig, Germany

Edited by Axel T. Brunger, Stanford University, Stanford, CA, and approved June 19, 2014 (received for review December 18, 2013)

Over the past 20 years, it has been widely accepted that membrane fusion proceeds via a hemifusion step before opening of the productive fusion pore. An initial hourglass-shaped lipid structure, the fusion stalk, is formed between the adjacent membrane leaflets (*cis* leaflets). It remains controversial if and how fusion proteins drive the subsequent transition (expansion) of the stalk into a fusion pore. Here, we propose a comprehensive and consistent thermodynamic understanding in terms of the underlying free-energy landscape of stalk expansion. We illustrate how the underlying free energy landscape of stalk expansion and the concomitant pathway is altered by subtle differences in membrane environment, such as leaflet composition, asymmetry, and flexibility. Nonleaky stalk expansion (stalk widening) requires the formation of a critical *trans*-leaflet contact. The fusion machinery can mechanically enforce *trans*-leaflet contact formation either by directly enforcing the *trans*-leaflets in close proximity, or by (electrostatically) condensing the area of the *cis* leaflets. The rate of these fast fusion reactions may not be primarily limited by the energetics but by the forces that the fusion proteins are able to exert.

hemagglutinin | SNARE | hemi | diaphragm | neuronal

Membrane fusion is a fundamental process in cell biophysics, being involved in viral infection, endo- and exocytosis, and fertilization. The textbook example of membrane fusion comprises three experimentally observed metastable lipidic structures—namely, the rhombohedral stalk (1, 2), the hemifusion diaphragm (HD) (3–5), and the toroidal fusion pore (6). These structures represent (local) free energy minima that are connected via transient states (free energy barriers) within the fusion pathway. How the stalk transitions (expands) into the fusion pore remains controversial (7–9). Different pathways have been proposed based on experimental observations (3, 5, 10–13), molecular simulations (8, 9, 14–20), continuum elastic models (15, 21, 22), and self-consistent field theory (23, 24).

Arguably, the best-studied fusion reactions are the ones mediated by influenza hemagglutinin and soluble *N*-ethylmaleimide-sensitive-factor attachment receptor (SNARE) molecules. Hemagglutinin-mediated fusion displays an unusual sensitivity toward point mutations in its amphiphilic fusion peptide. Here, even single point mutations can selectively trap the fusion reaction in a hemifused state (25). Hemagglutinin therefore very likely plays an active, essential role in the subsequent evolution of hemifusion intermediates (20). In contrast, it remains unclear if SNARE molecules play a role therein. SNARE molecules subject force on the membrane via the ends of the transmembrane domains (TMDs) (26). The X-ray–resolved structure of the postfusion neuronal SNARE complex suggests that TMDs come together during the fusion reaction, and may actively drive fusion up to the expansion of the fusion pore (27). However, in vitro and in vivo experiments, where the TMD was either replaced by a lipid anchor or partly truncated, provided mixed results concerning the essence of subsequent driving forces after initial membrane merger (28, 29).

To discern whether the fusion machinery plays an active role after stalk formation, we estimated the lower bound of the free energy barrier against expansion of the stalk. If stalk expansion faces a substantial free-energy barrier even under extremely fusogenic conditions (i.e., the lower bound of the free energy barrier), then fast, in vivo fusion reactions, such as synaptic fusion, likely involve an active mechanism.

We performed coarse grained molecular dynamics simulations, where computational efficiency is enhanced by representing several atoms by a single interaction site, to study the progression of a stalk formed between two highly curved "dimples" with a curvature of $-1/10$ nm^{-1}. We modeled such a scenario by studying the fusion process of a 20-nm–sized vesicle with its own periodic image (Fig. 1). Such an extreme curvature approaches the upper bound of membrane curvature that fusion proteins, such as synaptotagmin, can generate when being overexpressed on the membrane (30). The exaggerated curvature stress of the here-modeled fusion site should approach the lower bound of the in vivo expansion barrier (31, 32). In addition, we explored the effect of phosphatidylethanolamine (PE) lipids and cholesterol, the two abundant "fusogens" in the plasma membrane, on the expansion of the metastable stalk.

In total we performed more than 500 simulations of 1.6 μs each to study four relevant scenarios: (*i*) The leaflets of the surrounding bulk membrane are in equilibrium and material freely flows between the bulk membrane and the dimple; (*ii*) the flow of material between the dimple's cap and the surrounding bulk membrane is restricted/inhibited due to the crowding of nearby fusion proteins; (*iii*) a tension difference between the leaflets is induced by, e.g., an asymmetric ion concentration; and (*iv*) the presence of shape-stabilizing matrix proteins on the *trans*-leaflets of viral envelopes (11) or a membrane adhered to a solid support (supported bilayers).

To estimate the free energy required for (protein-mediated) expansion of the stalk, we placed a hydrophilic probe consisting of eight bundled solvent beads in each vesicle. We alter the equilibrium distance between the probes within the simulations (Fig. 2 and *SI Appendix, Methods*). Such a scenario mimics, e.g., the hydration shell(s) of the charged TMD ends (C termini) of

Significance

We focus on computing lipidic fusion pathway energetics and interpret them in a biological context. We illustrate that the progression of fast synaptic fusion may not rely on the point-like forces that are being transmitted to the membrane via the transmembrane domains of SNARE molecules. Our work bridges the many present gaps between diverse but related experiments and their interpretation, thus providing a coherent and integrative picture.

Author contributions: H.J.R. and H.G. designed research; H.J.R. and G.B. performed research; H.J.R., G.B., and H.G. analyzed data; and H.J.R., G.B., and H.G. wrote the paper.

The authors declare no conflict of interest.

This article is a PNAS Direct Submission.

[1]To whom correspondence should be addressed. Email: hrissel@gwdg.de.

This article contains supporting information online at www.pnas.org/lookup/suppl/doi:10.1073/pnas.1323221111/-/DCSupplemental.

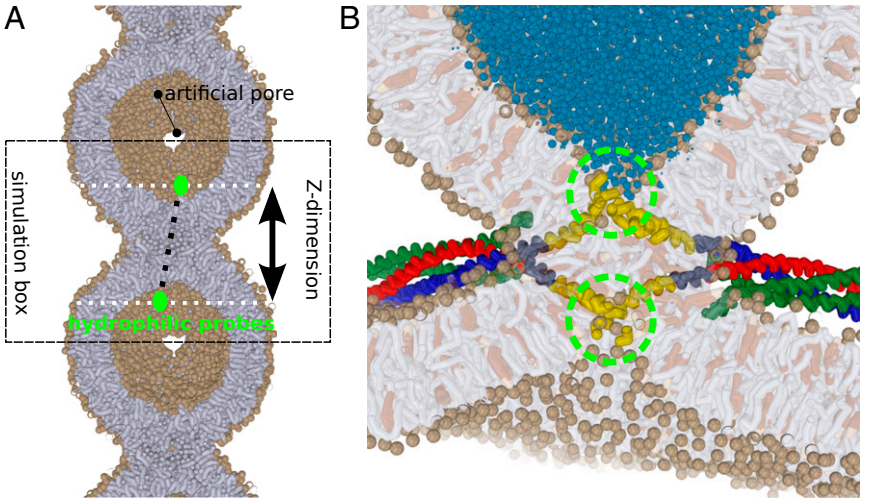

Fig. 1. (*A*) A 20-nm–sized vesicle, mimicking the protein-free cap of a (protein) induced dimple or nipple, fuses with its own periodic image. To ensure free flow of lipid material (tensionless conditions), two artificial pores with a radius 1.6 nm are present at the vesicle's foot. The simulation box can freely adjust its length in the Z dimension, as well as in the XY dimension. The green circles depict the hydrophilic probes which mimic the squeezing action of one or multiple SNARE complexes. (*B*) Example of a scenario where widening of the stalk is driven by the presence of multiple neuronal SNARE complexes (26, 51). The C termini of the transmembrane domains (green circles) exert a squeezing force on both the *trans*-leaflets and thereby drive thinning and widening of the stalk. Lipids: tails are shown in gray, head groups (spheres) in tan, cholesterol in brown. SNAREs: syntaxin-1A in red, synaptobrevin-2 in green, and SNAP-25 in green. Transmembrane domains are shown in yellow.

SNARE molecules (Fig. 1*B*) that come together during the fusion reaction (27), and thereby exert a squeezing force on the stalk (26).

First, we considered a scenario where the leaflets of the dimple are in equilibrium and the chemical potential of the *cis* and *trans*-leaflets remains constant during the fusion process. Free lipid exchange is facilitated between all four leaflets by placing two artificial 1.6-nm–sized pores at the foot of the dimple, which facilitate a lipid flip-flop rate of 0.4 ns^{-1} (33, 34) (Fig. 1*A* and *SI Appendix*, Fig. S1). Because the pores allow a free exchange of lipids and solvent, and because the x-, y-, and z-dimensions of the simulation box are semi-isotropically coupled to the same external pressure bath (1 bar), we can assume no lateral tension is present in the leaflets.

The Barrier of Nonleaky Dimple Stalk-Widening Is Independent of a Molecule's Spontaneous Curvature

We computed the free energy (potential of mean force) that is required to facilitate widening of the stalk by using umbrella sampling (*SI Appendix, Methods*). Fig. 2 shows the free energy as a function of probe-to-probe distance. Each point in the plot represents a separate 1.6-μs simulation performed at a constant probe to probe distance. The probes optimize their location such that the free energy is minimized at the given distance. We emphasize that we only restrained the z-dimension of the vector connecting the two probes, i.e., the dimension parallel to the central symmetry axis through the stalk. Therefore, the probes can move independently within the xy-plane—i.e., the plane perpendicular to the stalk's symmetry axis. The actual distance between the probes in three dimensions is therefore irrelevant. In this way, we do not impose radial symmetry when forcing the probes together, because the probes can penetrate the stalk anywhere at any angle, and thus the reaction pathway is not confined to the central symmetry axis through the stalk. The cited probe–probe distance is the distance along the z-dimension.

Decreasing the distance between the probes eventually forces the stalk to expand. The obtained fusion pathway resembles the hypothesized standard stalk–hemifusion pathway that proceeds through the nonleaky formation of an HD (22, 23). The plateau in the free energy profile below 6.5 nm distance (Fig. 2, III) indicates that subsequent stalk widening and pore formation occurs spontaneously, without the need of additional external work. Here, the relaxation of the dimple's curvature stress drives the subsequent expansion of the stalk. A detailed analysis of the

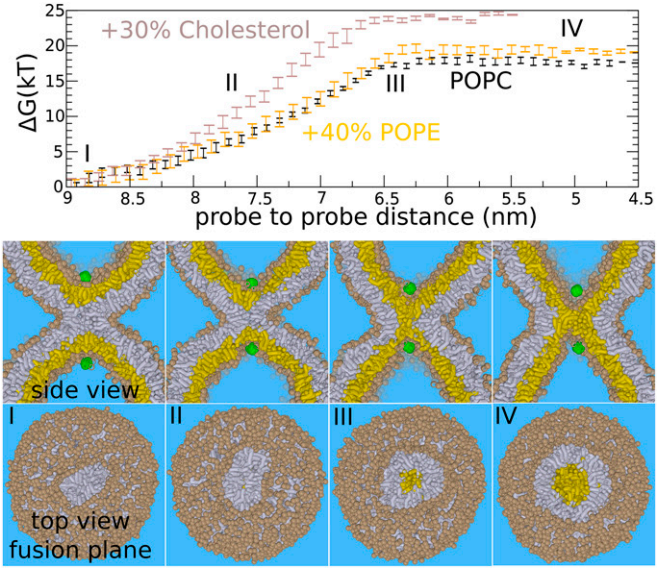

Fig. 2. The expansion barrier of the stalk—standard hemifusion mechanism. The figures show the fusion reaction between the membranes (at 310 K) in response to pulling two hydrophilic probes (green) toward each other through the center of the stalk. This process mimics the action of SNARE zipping where the hydrophilic transmembrane domain C termini are pulled together. (*Upper*) The required free energy for facilitating such a process. (*Lower*) Corresponding formation of the hemifusion diaphragm. The initial stalk (I) expands linearly (II) before expanding radially (III and IV). Once the barrier (III) of 17–24 k_BT is overcome, the subsequent formation/expansion of the hemifusion diaphragm (IV) becomes spontaneous (plateau region). The addition of 40% POPE does not significantly affect the barrier of stalk widening. The addition of 30% cholesterol marginally increases the barrier against stalk widening (from 17 to 24 k_BT). *Trans*-leaflets are shown in yellow, *cis* leaflets in gray. The example shows the situation for the pure POPC membrane (PC head groups are shown in tan).

cross-sectional shape, area, and circumference of the stalk as well as the decomposition of the free energy for stalk widening is shown in *SI Appendix*, Figs. S4–S7.

In agreement with self-consistent field (SCF) theory (23), the barrier features a structure where the *trans*-leaflets have formed an initial, critical contact that we will refer to as a critical *trans*-leaflet contact (TLC) (35) for simplicity. For a pure 1-palmitoyl-2-oleoylphosphatidylcholine (POPC) membrane, a free energy barrier of ∼17 k_BT (at 310 K) against nucleated stalk widening (HD formation) is obtained (Fig. 2, III).

It is important to note that the rate of fusion is not limited only by the energetics but also by the force that the fusion proteins are able to exert. For example, nucleation of stalk widening requires a relatively small contraction of the two probes, i.e., the distance between the probes decreases from ∼8.3 to 6.5 nm. This short nucleation regime of 1.8 nm, corresponding to a barrier of 17 k_BT (73 pN·nm), implies a substantial average pulling force of ∼40 pN. For comparison, optical tweezers experiments, where the isolated four-helix bundle SNARE complex was reversibly unfolded, suggested that coiled-coil formation in the SNARE complex generates pulling forces of up to 20 pN (36). Such a pulling force would imply that stalk widening is still opposed by a remaining thermal activation barrier of ∼10 k_BT even though the total work that the SNARE complex can perform, ∼40 k_BT, would suffice (36).

Once the expansion barrier is overcome, the additional free energy required to penetrate and rupture the formed hemifusion diaphragm is only a few k_BT, as indicated by the observation of spontaneous rupture in our simulations (*SI Appendix*, Fig. S3). We note, however, that the barrier against rupture depends on the HD's size (26), membrane composition (*SI Appendix*, Fig. S3), shape/topology (37), and concomitant tension (18).

The presynaptic plasma membrane is highly enriched with sterols (up to 60%) and PE lipids (40%) (38). We studied the effect of PE lipids (POPE) and cholesterol on the barrier against HD formation. We applied a parameterized model of cholesterol that has been shown to capture the liquid disorder to liquid order (lipid rafts) phase transition (39). With this simulation model, we have previously demonstrated the enhanced affinity of both PE lipids and cholesterol for the inner and thus negatively curved monolayer of a 20-nm–sized vesicle (34, 40).

The presence of 40% POPE did not significantly alter the expansion barrier (41) (Fig. 2). We note that PE headgroups are not expected to (further) enhance stalk widening if fusion (readily) occurs between two highly curved membranes (see *SI Appendix*, Figs. S4–S7 for detailed analysis). The presence of 30% cholesterol, in contrast, even increased the barrier against widening of the stalk—from 17 k_BT to ∼24 k_BT. Because these results may seem counterintuitive, we emphasize that the classification fusogen is derived from the molecules' ability to enhance initial lipid mixing (stalk formation) rather than stalk expansion. Recent X-ray studies suggest that these molecules enhance stalk formation mainly by lowering the energetic cost of leaflet approach (i.e., the hydration repulsion) (2).

The formation of the critical TLC involves an overall shape deformation in the dimple where the *trans*-leaflets adopt a narrow, pinched, hourglass shape (Fig. 2, III, and *SI Appendix*, Fig. S2). The presence of 30% cholesterol, which increases the elastic moduli of the POPC membrane, opposes the membrane's ability to adapt such conformation. This effect is illustrated by the increased slope (force) in the free energy profile (Fig. 2). Thus, dimple stalk widening requires membrane flexibility, but is rather unaffected by the spontaneous curvature of lipid molecules.

POPE but Not Cholesterol Enhances a Leaky Elongation of the Stalk

Recent molecular simulation studies and SCF have suggested that the progression of the stalk into the fusion pore can also proceed through pathways that are characterized by an asymmetric stalk expansion (stalk elongation). These pathways may lead to alternative formation of an HD (8, 14, 24), and associate the progression of fusion with the transient leakage observed in experiments (10, 11, 41). In our simulations, such a process can be triggered by placing one of the hydrophilic probes outside the dimple. We restrained the distance between the probes in three dimensions. The cited probe–probe distance is the length of the connecting distance vector. Fig. 3 shows that pulling the probes toward each other induced a leakage pore in the direct stalk vicinity. Because of the unfavorable excess free energy of a pore's rim (line tension), the stalk rapidly encircles the pore (stalk elongation) resulting in an alternative formation of an HD (20, 24).

From our umbrella simulations, such a leaky mechanism faces a barrier of ∼35 k_BT (pure POPC, 310 K). This barrier is due to the required formation of the leakage pore, and the subsequent fusion reaction occurs spontaneously once the leakage pore is formed (Fig. 3, III) (14). We emphasize that elongation of the stalk is spontaneous in the inverted hexagonal phase regime, i.e., in the presence of a very high (local) PE or cholesterol concentration (24, 26, 42). Such a progression of a stalk may result in a "double" HD (*SI Appendix*, Fig. S11)—i.e., an inverted micelle intermediate (24, 26), which is believed to be formed in homotypic vacuole fusion (13). For the here-studied membrane compositions, however, stalk elongation is not spontaneous; rather, it results from the free energy reduction due to the nearby membrane perturbation, i.e., the probes that locally thin the membrane (negative hydrophobic mismatch). This effect is evidenced by an observed attraction between stalk and perturbation.

Next, we studied the effect of POPE and cholesterol on the barrier against a leaky stalk expansion. The addition of 40% POPE

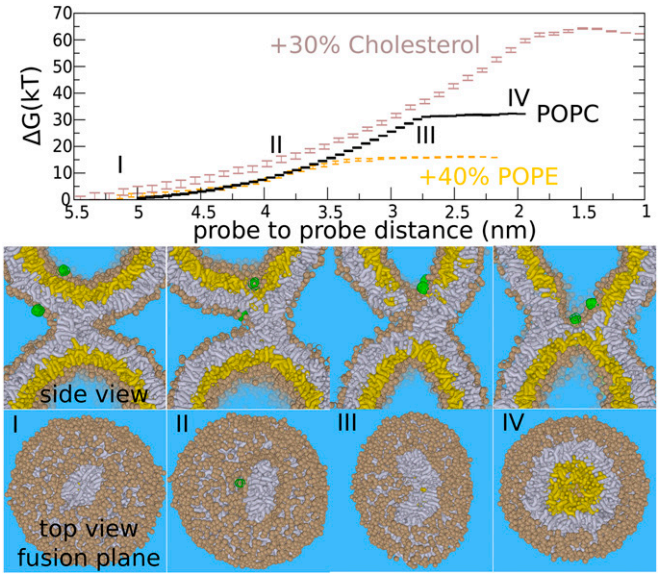

Fig. 3. The expansion barrier of the stalk—leaky stalk expansion. Figures show the fusion reaction between the membranes (at 310 K) in response to pulling two hydrophilic probes (green) toward each other. A leaky hemifusion mechanism (via elongation of the stalk) results after placing one of the probes outside the vesicle. (*Upper*) Required free energy for facilitating such a process. (*Lower*) Corresponding formation of the hemifusion diaphragm. The barrier in this pathway is the nucleation of a leakage pore (III). The addition of 40% POPE (orange) lowers the barrier of the leaky mechanism to ∼17 k_BT but does not significantly affect the barrier in the standard hemifusion mechanism. The addition of 30% cholesterol (brown) strongly increases the barrier of the leaky pathway (35–64 k_BT). *Trans*-leaflets are shown in yellow, *cis* leaflets in gray. The example shows the situation for the pure POPC membrane (PC head groups are shown in tan).

reduced the barrier of the stalk–pore nucleation transition by 50%, from ∼35 to 15 k_BT (Fig. 2). Thus, PE lipids strongly enhance leaky fusion, which is in agreement with SCF theory (24). In contrast, cholesterol increased the barrier against a leaky stalk expansion in our simulations from ∼35 to 64 k_BT (Fig. 3). This observation implies that, in the presence of 30% cholesterol, the leaky mechanism is energetically outperformed by nonleaky widening of the stalk (64 vs. 24 k_BT) (43). It is thus essential to stress that fusogens with a very similar negative spontaneous curvature, such as DOPE and cholesterol, promote the stalk to fusion pore transition via distinct pathways. More relevant than the spontaneous curvature is the molecule's ability to facilitate stalk elongation vs. stalk bending, and is illustrated in detail in *SI Appendix*, Fig. S8.

Nonleaky Stalk Widening, but Not Leaky Stalk Elongation, Crucially Depends on the Ability of Both *Trans*-Leaflets to Stretch and Bend

The following section investigates scenario *ii*, were the lipid flow between the dimples and surrounding bulk membrane is effectively restricted/inhibited on the time scale of membrane fusion, which mimics the crowding of nearby fusion proteins, the absence of flip-flops, and the finite size of the synaptic vesicle's inner leaflet. The inability to equilibrate the chemical potential of the monolayers during the fusion reaction may impair the formation of crucial intermediates, such as a TLC, where the dimples collectively stretch and bend into a narrow, pinched, hourglass shape (Fig. 2, III, and *SI Appendix*, Fig. S2). To mimic this scenario, we recalculated the free energy barrier against (nonleaky) stalk widening in a pure POPC system without artificial pores, thereby conserving the population of the monolayers. Here, we used an initially equilibrated dimple/vesicle, where we define equilibrium as the absence of net lipid flow between the leaflets under presence of artificial pores (33). We observed that the barrier against stalk widening increases by ∼5 k_BT (22 k_BT). Thus, for two dimples consisting of ∼1,100 lipids each, a fixed lipid population (finite size effect) is expected to alter the barrier against stalk widening only slightly. This observation is supported by the apparent absence of a net lipid flow between the leaflets up to barrier crossing in the scenario *i* umbrella simulations with artificial pores (*SI Appendix*, Fig. S1).

How then does the expansion barrier depend on the (population) asymmetry of the leaflets (i.e., the spontaneous curvature of the bilayer)? To answer this question, we recalculated the barrier against stalk widening using a self-formed (33) vesicle that has 33 lipids more in the *cis* leaflet (2.3%) and 33 lipids less in the *trans*-leaflet (4.1%). In contrast to the previous simulations, however, we did not additionally equilibrate this vesicle by introducing artificial pores. Strikingly, for such a nonequilibrated vesicle/dimple, the barrier against stalk widening is ∼30 k_BT higher than for the equilibrated vesicle (Fig. 4 *A* and *C*). In contrast, the barrier against the leaky pathway is similar for both systems, ∼35 k_BT (Fig. 4*B*), and thus seems rather unaffected by the altered membrane asymmetry. Both trends are also seen for different lipid compositions (Fig. 4*B*). Thus, these observations underscore the importance of vesicle equilibration, an issue that to the best of our knowledge has thus far not been explicitly taken into account in molecular fusion simulation studies or in experimental vesicle fusion assays, and which may be able to explain various discrepancies in the literature (7–9). We further emphasize that the

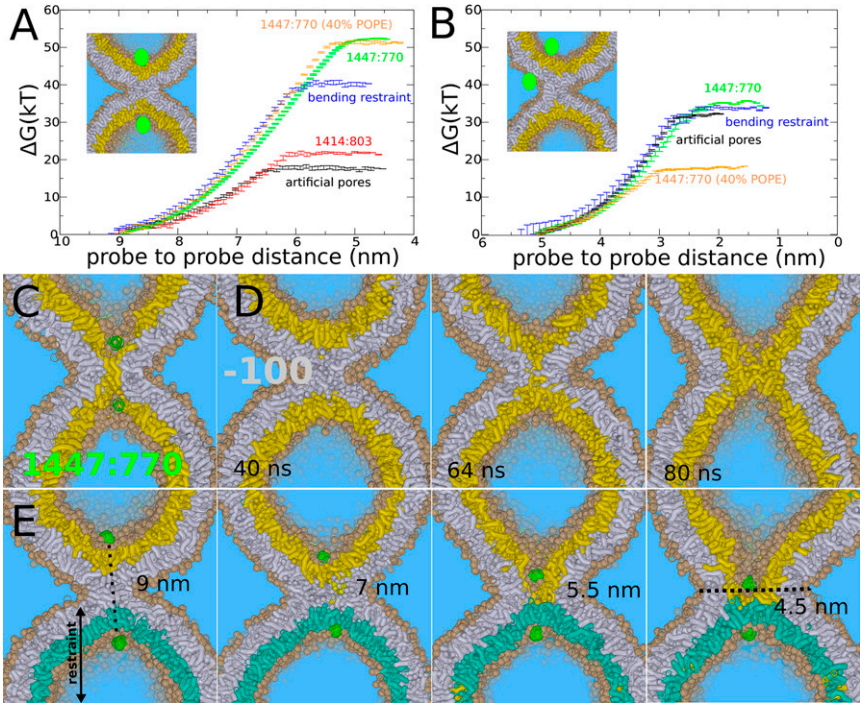

Fig. 4. Stalk expansion for the POPC vesicle under various constraints. (*A*) Barrier against stalk widening for a vesicle with artificial pores (black line), an initially equilibrated vesicle with 1,414 lipids in the *cis* leaflet and 803 lipids in the *trans*-leaflet (red line), a vesicle with artificial pores but with a bending restraint on one of the *trans*-leaflets (blue line), a vesicle formed by spontaneous aggregation (1,447:770) without additional equilibration (green line), 1,447:770 with 40% POPE (orange line). (*B*) Barrier against leaky stalk elongation for a vesicle with artificial pores (black line), a vesicle with artificial pore but with a bending restraint on one of the *trans*-leaflets (blue line), vesicle formed by spontaneous aggregation (1,447:770) without additional equilibration (green line), 1,447:770 with 40% POPE. (*C*) *Trans*-leaflet contact, the barrier in stalk widening, formed in the nonequilibrated vesicle (1,447:770). (*D*) Rapid, spontaneous widening of stalk after removal of 100 lipids from the *cis* leaflet, mimicking an induced area condensation of ∼7%. (*E*) Stalk widening in the presence of a bending restraint on one of the *trans*-leaflets (cyan) mimicking the presence of a shape-stabilizing protein matrix or bilayer support. The center of the formed hemifusion diaphragm is not aligned with the center of the *cis* leaflets (black dotted line).

presence of cholesterol, despite its ability to laterally redistribute itself, does not prevent these asymmetry effects (see *SI Appendix*, Fig. S9 for a detailed analysis).

Alterations in membrane asymmetry, however, can also enhance stalk widening. For example, the addition of divalent cations to the exterior solvent has been used in several in vitro assays to induce hemifusion and the subsequent expansion of the hemifusion diaphragm between giant unilamellar vesicles (3). These divalent cations alter membrane tension by condensing negatively charged lipid membranes electrostatically, e.g., Ca^{2+} reduces the *cis* leaflet area by 5–7%, depending on concentration and membrane composition (44). We stress that such an induced tension is asymmetric and enforces an area condensation specifically in the outer *cis* leaflets of the liposomes where the ions are present (creating interleaflet tension) (45, 46).

To simulate such an effect, we removed 100 lipids from the *cis* leaflet, which corresponds to a relevant area condensation of 7%; intriguingly, this facilitates spontaneous stalk widening within 100 ns in our simulations (Fig. 4*D*). This result demonstrates the strong inherent driving force of such an area condensation in the *cis* leaflet, which agrees with recent (combined) experimental and theoretical work (3, 46). We conclude that stalk widening is promoted by tension in the *cis* leaflets or equivalently an excess of membrane material in the *trans*-leaflets, and is impaired by the presence of tension in the *trans*-leaflets or equivalently insufficient membrane material. We note that these two scenarios respectively facilitate or hinder stretching/bending of the *trans*-leaflets that is required to form the critical TLC intermediate (Fig. 4*C*).

Our results suggest that in vitro fusion setups, where fusion is subject to an artificially induced interleaflet tension, underestimate the intrinsic nucleation barrier against stalk expansion. However, the (asymmetric) release of calcium in the presence of negatively charged lipids, such as phosphatidylserine and phosphatidylinositol 4,5-bisphosphate, may be an important strategy to selectively enhance nonleaky stalk widening in synaptic fusion.

Recent electron cryotomography studies revealed that the influenza virus envelope remains essentially unperturbed during leaky fusion with a pure DOPC liposome (11). The M1 matrix layer of the influenza envelope serves as an endoskeleton for the virus and a foundation for hemagglutinin during membrane fusion (11). To study the effect of shape-stabilizing matrix proteins or an equivalent adhesive membrane support (supported membranes) (41), we restricted the bending of one of the *trans*-leaflets (*SI Appendix*). We reintroduced the two artificial pores, so that the lipids in the unrestrained *trans*-leaflets can freely flip-flop and diffuse. Fig. 4*E* shows the process of stalk widening in the presence of this restraint. It is intuitive that such an asymmetric formation of a critical TLC is accompanied by an increased free energy barrier. Indeed, we obtained a barrier of 40 k_BT, and thus an increase of 23 k_BT, for the pure POPC system (Fig. 4*A*). We note that this barrier very likely increases when the curvature of the restrained leaflet decreases, because this would further challenge formation of the narrow pinched TLC. In contrast, we observed that the barrier of leaky stalk expansion, where a pore was formed on the opposite, unrestrained leaflet, is not affected by the presence of such a bending restraint (Fig. 4*B*). Thus, our simulations suggest that stabilizing membrane shape selectively opposes nonleaky stalk widening, in agreement with the observation of a predominantly leaky fusion reaction in the experiments (11).

On the Cutting Edge of Membrane Fusion

To summarize, we mimicked a scenario where the fusion machinery has already performed a considerable amount of work to induce strong membrane curvature as well as the initial stalk. The elastic bending moduli of these model membranes are likely close to the upper bound of the experimentally derived regime (47). The high curvature stress stored in the membranes enhances expansion of the stalk (15, 32, 48); however, a significant free energy barrier against nonleaky widening of the stalk remains.

We further illustrated that nonleaky fusion competes with leaky fusion. The membrane composition strongly affects the (lower bound) expansion barrier of stalk elongation (leaky fusion) but not that of stalk widening (nonleaky fusion). The latter seems solely related to the elastic membrane deformations required to form a critical contact between the *trans*-leaflets. Recent X-ray studies and simulations revealed that both the width and shape of the (rhombohedral) stalk are rather independent of hydration level (intermembrane distance) and membrane composition (2, 49). These observations further support that widening of the stalk faces a free energy barrier and is not easily enhanced by tuning the lipid composition or forcing membranes in closer proximity.

However, one may tune the (local) membrane composition such that expansion of the stalk, via elongation, faces a very small barrier up to the point that it eventually occurs spontaneously, which would lead to the formation of an inverted micelle intermediate in vesicle–vesicle fusion (13, 24, 26). Therefore, it is not only the barrier against expansion of the stalk that forms a challenge in synaptic fusion, it is rather the requirement of both a fast (within milliseconds) and exclusively nonleaky fusion reaction.

The fusion machinery can actively enforce such a reaction in two ways: (*i*) It can enforce close proximity of the *trans*-leaflet by subjecting a point-like force on the leaflet, for example, via the transmembrane domains of fusion proteins, or (*ii*) it can actively condense the *cis* leaflets near the fusion site, for example, via the condensation of negatively charged lipids in the presence of Ca^{2+}. We emphasize that synaptic fusion is triggered by the asymmetric release of calcium (5). Here, the presence of the positively charged SNARE linkers (50), which reside near the lipid head groups (Fig. 1), may additionally contribute to such an electrostatic condensation. Interestingly, replacement of the membrane spanning TMDs of synaptic SNARE molecules by lipid molecules did not disrupt synaptic transmission in recent in vivo whole-cell patch-clamp experiments (29). In such a scenario, the SNAREs were unable to actively pull the *trans*-leaflets via the TMD ends and thereby enforce nonleaky stalk widening, which suggests that the fast synaptic fusion machinery may involve (local) condensation of the *cis* leaflets to enforce widening of the stalk.

We illustrated that the rate of a fusion reaction may not be primarily limited by the energetics but by the point-like forces that the fusion proteins are able to exert. To expand the stalk, the ∼4-nm-long SNARE TMDs should transmit a substantial downward force to the C termini while being under a 120° angle (Fig. 1*B*) and despite the presence of semiflexible linkers (26). Due to reasons of mechanical efficiency, it is thus very likely that only a fraction of the experimentally estimated 20 pN (36), which is generated by the coiled-coil complex, is being transmitted to the TMD ends. Progression of fast (millisecond) synaptic fusion may not rely on these generated forces; rather, it involves alternative mechanisms for fast synchronous release such as, e.g., electrostatic condensation of the *cis* leaflets; this may explain why replacement of TMDs by lipid molecules does not affect synaptic release (29). To form a fusion pore, however, the expanding stalk/HD should rupture and dilate before expanding toward a metastable size (3, 5, 26). Recent in vitro experiments suggest that a timed interplay between SNARE molecules, Complexin and Synaptotagmin-1 ensures fast fusion pore formation and prevents formation of metastable HDs (5).

Finally, within our definition of leaky fusion, some nuances should be noted. The leakage pores observed in fusion simulations with tensionless membranes (8, 9, 20) are typically less than 2 nm in diameter with lifetimes of only up to hundreds of nanoseconds. Notably, we have observed similar small, short-lived pores in our simulations of SNARE-mediated fusion (26,

51) (*SI Appendix*, Fig. S12). Considering the small sizes and submicrosecond lifetimes of these leaky pores, it is uncertain if experiments would classify these pathways as being leaky. Leakage pores as pores in general, however, are expected to become larger and longer-lived, and thus more detectable, when the membrane(s) are under tension. Alternatively, our simulations (20) suggest that leakage pores can become metastable in the presence of amphiphilic fusion peptides, which line such a pore and thereby hinder "closing" of the elongated stalk (*SI Appendix*, Fig. S13). Such metastability is supported by the observation of very similar leaky fusion intermediates in recent electron cryotomography studies of influenza fusion (11). It is thus plausible that the leaky fusion observed in experiments often results from hindrance or misguidance of the fusion reaction by fusion proteins (52).

Methods and S-enumerated figures are provided in *SI Appendix*.

ACKNOWLEDGMENTS. We thank Reinhard Jahn, Michael Schick, Marcus Müller, and Yuliya Smirnova for stimulating discussions and constructive comments. Financial support was provided by Deutsche Forschungsgemeinschaft Grant SFB 803.

1. Yang L, Huang HW (2003) A rhombohedral phase of lipid containing a membrane fusion intermediate structure. *Biophys J* 84(3):1808–1817.
2. Aeffner S, Reusch T, Weinhausen B, Salditt T (2012) Energetics of stalk intermediates in membrane fusion are controlled by lipid composition. *Proc Natl Acad Sci USA* 109(25):E1609–E1618.
3. Nikolaus J, Stöckl M, Langosch D, Volkmer R, Herrmann A (2010) Direct visualization of large and protein-free hemifusion diaphragms. *Biophys J* 98(7):1192–1199.
4. Hernandez JM, et al. (2012) Membrane fusion intermediates via directional and full assembly of the SNARE complex. *Science* 336(6088):1581–1584.
5. Diao J, et al. (2012) Synaptic proteins promote calcium-triggered fast transition from point contact to full fusion. *eLife* 1:e00109.
6. Haluska CK, et al. (2006) Time scales of membrane fusion revealed by direct imaging of vesicle fusion with high temporal resolution. *Proc Natl Acad Sci USA* 103(43): 15841–15846.
7. Chernomordik LV, Kozlov MM (2008) Mechanics of membrane fusion. *Nat Struct Mol Biol* 15(7):675–683.
8. Schick M (2011) Membrane fusion: The emergence of a new paradigm. *J Stat Phys* 142:1317–1323.
9. Markvoort AJ, Marrink SJ (2011) Lipid acrobatics in the membrane fusion arena. *Curr Top Membr* 68:259–294.
10. Frolov VA, Dunina-Barkovskaya AY, Samsonov AV, Zimmerberg J (2003) Membrane permeability changes at early stages of influenza hemagglutinin-mediated fusion. *Biophys J* 85(3):1725–1733.
11. Lee KK (2010) Architecture of a nascent viral fusion pore. *EMBO J* 29(7):1299–1311.
12. Wang L, Seeley ES, Wickner W, Merz AJ (2002) Vacuole fusion at a ring of vertex docking sites leaves membrane fragments within the organelle. *Cell* 108(3):357–369.
13. Wickner W (2010) Membrane fusion: Five lipids, four SNAREs, three chaperones, two nucleotides, and a Rab, all dancing in a ring on yeast vacuoles. *Annu Rev Cell Dev Biol* 26:115–136.
14. Müller M, Katsov K, Schick M (2003) A new mechanism of model membrane fusion determined from Monte Carlo simulation. *Biophys J* 85(3):1611–1623.
15. Kuzmin PI, Zimmerberg J, Chizmadzhev YA, Cohen FS (2001) A quantitative model for membrane fusion based on low-energy intermediates. *Proc Natl Acad Sci USA* 98(13): 7235–7240.
16. Kasson PM, et al. (2006) Ensemble molecular dynamics yields submillisecond kinetics and intermediates of membrane fusion. *Proc Natl Acad Sci USA* 103(32):11916–11921.
17. Kasson PM, Pande VS (2007) Control of membrane fusion mechanism by lipid composition: Predictions from ensemble molecular dynamics. *PLoS Comput Biol* 3(11): 2228–2238.
18. Grafmüller A, Shillcock J, Lipowsky R (2009) The fusion of membranes and vesicles: Pathway and energy barriers from dissipative particle dynamics. *Biophys J* 96(7): 2658–2675.
19. Lindau M, Hall BA, Chetwynd A, Beckstein O, Sansom MS (2012) Coarse-grain simulations reveal movement of the synaptobrevin C-terminus in response to piconewton forces. *Biophys J* 103(5):959–969.
20. Risselada HJ, et al. (2012) Line-tension controlled mechanism for influenza fusion. *PLoS ONE* 7(6):e38302.
21. Siegel DP (1993) Energetics of intermediates in membrane fusion: Comparison of stalk and inverted micellar intermediate mechanisms. *Biophys J* 65(5):2124–2140.
22. Kozlovsky Y, Chernomordik LV, Kozlov MM (2002) Lipid intermediates in membrane fusion: Formation, structure, and decay of hemifusion diaphragm. *Biophys J* 83(5): 2634–2651.
23. Katsov K, Müller M, Schick M (2004) Field theoretic study of bilayer membrane fusion. I. Hemifusion mechanism. *Biophys J* 87(5):3277–3290.
24. Katsov K, Müller M, Schick M (2006) Field theoretic study of bilayer membrane fusion: II. Mechanism of a stalk-hole complex. *Biophys J* 90(3):915–926.
25. Qiao H, Armstrong RT, Melikyan GB, Cohen FS, White JM (1999) A specific point mutant at position 1 of the influenza hemagglutinin fusion peptide displays a hemifusion phenotype. *Mol Biol Cell* 10(8):2759–2769.
26. Risselada HJ, Grubmüller H (2012) How SNARE molecules mediate membrane fusion: Recent insights from molecular simulations. *Curr Opin Struct Biol* 22(2):187–196.
27. Stein A, Weber G, Wahl MC, Jahn R (2009) Helical extension of the neuronal SNARE complex into the membrane. *Nature* 460(7254):525–528.
28. Xu Y, Zhang F, Su Z, McNew JA, Shin YK (2005) Hemifusion in SNARE-mediated membrane fusion. *Nat Struct Mol Biol* 12(5):417–422.
29. Zhou P, Bacaj T, Yang X, Pang ZP, Südhof TC (2013) Lipid-anchored SNAREs lacking transmembrane regions fully support membrane fusion during neurotransmitter release. *Neuron* 80(2):470–483.
30. Martens S, Kozlov MM, McMahon HT (2007) How synaptotagmin promotes membrane fusion. *Science* 316(5828):1205–1208.
31. Malinin VS, Lentz BR (2004) Energetics of vesicle fusion intermediates: Comparison of calculations with observed effects of osmotic and curvature stresses. *Biophys J* 86(5): 2951–2964.
32. Lee JY, Schick M (2008) Calculation of free energy barriers to the fusion of small vesicles. *Biophys J* 94(5):1699–1706.
33. Risselada HJ, Mark AE, Marrink SJ (2008) Application of mean field boundary potentials in simulations of lipid vesicles. *J Phys Chem B* 112(25):7438–7447.
34. Risselada HJ, Marrink SJ (2009) Curvature effects on lipid packing and dynamics in liposomes revealed by coarse grained molecular dynamics simulations. *Phys Chem Chem Phys* 11(12):2056–2067.
35. Siegel DP (1999) The modified stalk mechanism of lamellar/inverted phase transitions and its implications for membrane fusion. *Biophys J* 76(1 Pt 1):291–313.
36. Gao Y, et al. (2012) Single reconstituted neuronal SNARE complexes zipper in three distinct stages. *Science* 337(6100):1340–1343.
37. Nishizawa M, Nishizawa K (2013) Molecular dynamics simulation analysis of membrane defects and pore propensity of hemifusion diaphragms. *Biophys J* 104(5): 1038–1048.
38. Takamori S, et al. (2006) Molecular anatomy of a trafficking organelle. *Cell* 127(4): 831–846.
39. Risselada HJ, Marrink SJ (2008) The molecular face of lipid rafts in model membranes. *Proc Natl Acad Sci USA* 105(45):17367–17372.
40. Risselada HJ, Marrink SJ, Müller M (2011) Curvature-dependent elastic properties of liquid-ordered domains result in inverted domain sorting on uniaxially compressed vesicles. *Phys Rev Lett* 106(14):148102.
41. Wang T, Smith EA, Chapman ER, Weisshaar JC (2009) Lipid mixing and content release in single-vesicle, SNARE-driven fusion assay with 1-5 ms resolution. *Biophys J* 96(10): 4122–4131.
42. Marrink SJ, Mark AE (2004) Molecular view of hexagonal phase formation in phospholipid membranes. *Biophys J* 87(6):3894–3900.
43. Connor J, Yatvin MB, Huang L (1984) pH-sensitive liposomes: Acid-induced liposome fusion. *Proc Natl Acad Sci USA* 81(6):1715–1718.
44. Uhríková D, Kučerka N, Teixeira J, Gordeliy V, Balgavý P (2008) Structural changes in dipalmitoylphosphatidylcholine bilayer promoted by ca(2+) ions: A small-angle neutron scattering study. *Chem Phys Lipids* 155(2):80–9.
45. Chanturiya A, Scaria P, Woodle MC (2000) The role of membrane lateral tension in calcium-induced membrane fusion. *J Membr Biol* 176(1):67–75.
46. Warner JM, O'Shaughnessy B (2012) The hemifused state on the pathway to membrane fusion. *Phys Rev Lett* 108(17):178101.
47. Hu M, de Jong DH, Marrink SJ, Deserno M (2013) Gaussian curvature elasticity determined from global shape transformations and local stress distributions: A comparative study using the MARTINI model. *Faraday Discuss* 161:365–382, discussion 419–459.
48. McMahon HT, Kozlov MM, Martens S (2010) Membrane curvature in synaptic vesicle fusion and beyond. *Cell* 140(5):601–605.
49. Daoulas KC, Müller M (2013) Exploring thermodynamic stability of the stalk fusion-intermediate with three-dimensional self-consistent field theory calculations. *Soft Matter* 9(15):4097–4102.
50. van den Bogaart G, et al. (2011) Membrane protein sequestering by ionic protein-lipid interactions. *Nature* 479(7374):552–555.
51. Risselada HJ, Kutzner C, Grubmüller H (2011) Caught in the act: Visualization of SNARE-mediated fusion events in molecular detail. *ChemBioChem* 12(7):1049–1055.
52. Südhof TC (2007) Membrane fusion as a team effort. *Proc Natl Acad Sci USA* 104(34): 13541–13542.